# Magnetic structures of Na$L$MnWO$_6$ perovskites ($L$=La,Nd,Tb)

Graham King,[1] Andrew S. Wills,[2] and Patrick M. Woodward[1]
[1]*Department of Chemistry, The Ohio State University, 100 West 18th Avenue, Columbus, Ohio 43210, USA*
[2]*Department of Chemistry, University College London, 20 Gordon Street, London WC1H 0AJ, United Kingdom*
(Received 13 November 2008; revised manuscript received 19 March 2009; published 24 June 2009)

The magnetic structures of the perovskites NaLaMnWO$_6$, NaNdMnWO$_6$, and NaTbMnWO$_6$, with rocksalt ordering of the Mn/W ions and layered ordering of Na and the rare-earth ions, have been determined by neutron powder diffraction. The manganese moments in NaLaMnWO$_6$ order below 10 K with a propagation vector of $\boldsymbol{k}_{14}=(\frac{1}{2},0,\frac{1}{2})$ and a moment of 3.99$\mu_B$ per $Mn^{2+}$ ion. The $Mn^{2+}$ and $Nd^{3+}$ ions order simultaneously in NaNdMnWO$_6$ at 11 K. The resulting magnetic structure is incommensurate with the underlying crystal structure and has the propagation vector of $\boldsymbol{k}_5=(0,0.48,\frac{1}{2})$. NaTbMnWO$_6$ undergoes two magnetic phase transitions at 15 and 9 K. The structure determined at 11 K is based on two propagation vectors of $\boldsymbol{k}_{14}=(\frac{1}{2},0,\frac{1}{2})$ and $\boldsymbol{k}_5=(0,0.427,\frac{1}{2})$. Upon cooling at 6 K the incommensurate vector is no longer present and the moments order only according to $\boldsymbol{k}_{14}$. The moments of the Nd and Tb ions are found to remain within the planes of the $A$-site cations, and in NaTbMnWO$_6$ the Mn moments also lie within the $xy$ plane. This study not only reveals magnetic structures with previously unexplored topologies but it also sheds light on the intricate coupling between the two magnetic sublattices.

DOI: 10.1103/PhysRevB.79.224428 PACS number(s): 75.30.Cr, 75.50.−y, 61.05.fm

## I. INTRODUCTION

Perovskites represent one of the most important classes of functional materials known, exhibiting a wide variety of technologically useful properties. There are numerous examples where the ordering of magnetic ions within the perovskite lattice leads to desirable properties. Examples include colossal magnetoresistance in $(Ca_xLa_{1-x})MnO_3$ and $(Sr_xLa_{1-x})MnO_3$ compounds[1–3] and half metallic transport in the ferrimagnetic double perovskite $Sr_2FeMoO_6$.[4–6] Perovskites have also played a leading role in multiferroics research. $BiFeO_3$ (Ref. 7) and $BiMnO_3$ (Ref. 8) are two of the more highly studied multiferroic materials. Many of the improper multiferroic materials that have been the subject of intense research efforts over the past few years are also perovskites.[9–11] In compounds such as $TbMnO_3$ (Refs. 12 and 13) and other $LMnO_3$ (Ref. 14) perovskites incommensurate spiral magnetic ordering has been found to induce a ferroelectric state that is much more strongly coupled to the magnetic order than in conventional multiferroics.

Recently, attention has been drawn to a relatively unexplored class of $AA'BB'O_6$ perovskites that exhibit ordering on both cation sublattices.[15,16] These compounds are interesting from a structural perspective in that they exhibit rocksalt ordering of the $B$-site cations and layered ordering of the $A$-site cations (see Fig. 1). The latter type of ordering was, until recently, very rare in stoichiometric perovskites. The availability of four distinct cation sites opens the door to the design of magnetic materials with novel topologies. Furthermore, compounds with this structure type show potential for multiferroic behavior by virtue of (a) relatively subtle coupling between two different magnetic sublattices and (b) their tendency to crystallize in polar space groups.

This study concerns the magnetic structures of three such compounds of the Na$L$MnWO$_6$ series with $L$=La, Nd, and Tb. All three compounds are known to undergo paramagnetic to antiferromagnetic (AF) transitions at low temperatures with Néel temperatures ($T_N$) ranging from 10–15 K.[16] The compounds with $L$=Nd or Tb are of particular interest because they possess layers of magnetic lanthanides separated by layers of nonmagnetic sodium ions superimposed with $Mn^{2+}$ cations on a pseudoface-centered-cubic (fcc) lattice. Furthermore, magnetic susceptibility measurements have indicated that NaTbMnWO$_6$ undergoes at least two magnetic phase transitions.[16] The magnetic structure of a compound with such an arrangement of magnetic ions has not been determined before and provides a basis for understanding the coupling that occurs between the rare-earth and transition-metal sublattices.

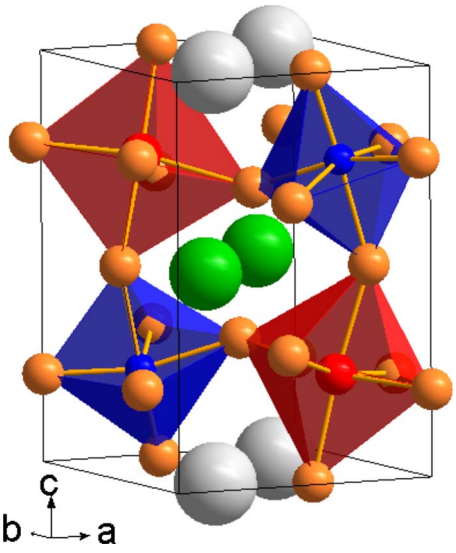


FIG. 1. (Color online) (a) The crystal structure of NaTbMnWO$_6$. Small blue (black) spheres are $W^{6+}$, small red (dark gray) spheres are $Mn^{2+}$, large light gray spheres are $Na^+$, large green (dark gray) spheres are $Tb^{3+}$, and small orange (light gray) spheres are $O^{2-}$.

 

## II. EXPERIMENTAL

The synthesis, crystal structures, and magnetic susceptibilities of these compounds have been previously reported and are described elsewhere.[16] Impedance measurements on sintered pellets of these materials have shown them to have resistivities on the order of $10^8$ Ω cm. Neutron powder diffraction (NPD) data were collected using the BT-1 32 detector neutron powder diffractometer at the NIST Center for Neutron Research (NCNR).[17] A Cu(311) monochromator with a 90° takeoff angle, $\lambda = 1.5403(2)$ Å, and in-pile collimation of 15 min of arc were used. Data were collected over the range of $3 \leq 2\theta \leq 168°$ with a step size of 0.05°.

Data sets were collected for all three compounds at (a) room temperature, (b) several degrees above $T_N$, and (c) below each transition temperature. For $NaLaMnWO_6$ low-temperature patterns were taken at 20 and ~5 K (averaged over the range of 5.1–7.3 K). For $NaNdMnWO_6$ low-temperature patterns were taken at 18 and ~4 K. For $NaTbMnWO_6$ low-temperature patterns were collected at 20, 11, and ~6 K (averaged over the range of 5.4–6.9 K). Indexing of the commensurate and incommensurate magnetic reflections was carried out using a new procedure developed in the program SARAH,[18] whereby for a given $k$ vector the moment orientations were refined using reverse–Monte Carlo (RMC) cycling. The trial propagation vectors were determined using a grid search of the points, lines, and planes of the Brillouin zone.[19] This technique was first developed for the study of incommensurate ordering in the frustrated magnet $\beta$-$Mn_{1-x}Ru_x$ (Ref. 20) and has many advantages over the conventional indexing algorithms based on the peak positions alone. These arise from the physical nature of the refinement process: magnetic intensity is only permitted in patterns that are possible for the moment positions in the cell, with a particular $k$ vector, and the choices of trial vectors is driven by the different translational symmetry types of the eigenfunctions of the exchange Hamiltonian.[21,22] That this technique only produces good fits where magnetic intensity can physically be produced thereby reduces the number of false positives that are obtained by conventional indexing based on the peak positions alone. No assumptions are made over the nature of the Hamiltonian or the exchange interactions as it also allows the sequential determination of structures with several unrelated propagation vectors, as is the case for $NaTbMnWO_6$.

Calculations of the different symmetry-allowed magnetic structures for a given propagation vector were done using the technique of representational theory[23–27] using SARAH. In all cases the refinements were carried out directly in terms of the linear summation of symmetry-adapted bases that are generated by the symmetry calculations, a technique that has been successfully applied to a variety of magnetic structures, such as those in the $M^{II}[N(CN)_2]_2$ molecular magnets,[28] the jarosites $AFe_3(SO_4)_2(OH)_6$ ($A = Na^+, K^+, NH_4^+, Ag^+, Rb^+$),[29] and the rare-earth pyrochlores.[30,31] This was achieved using SARAH together with GSAS (Refs. 32 and 33) for $NaLaMnWO_6$. As GSAS does not allow propagation vectors to define the translational symmetries of magnetic structures, the observation of incommensurate magnetic ordering in $NaNdMnWO_6$ and $NaTbMnWO_6$ required the use of an alternative Rietveld program. Therefore, SARAH and FULLPROF (Ref. 34) were used for these refinements.

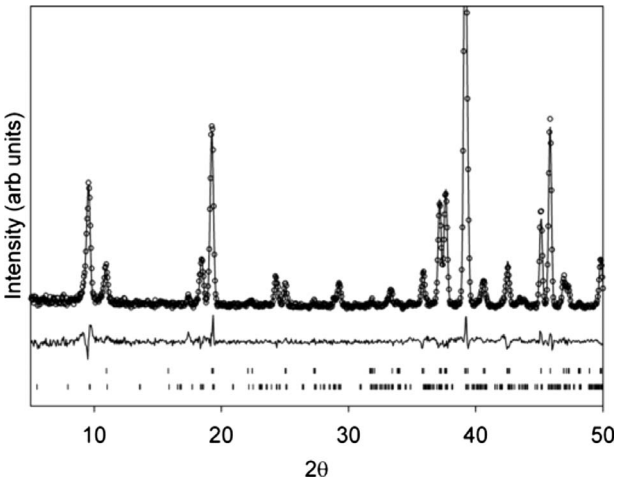


FIG. 2. The neutron powder diffraction spectrum of $NaLaMnWO_6$ obtained at 5 K using neutrons of wavelength 1.5403(2) Å. The observed data points are shown as open circles, the calculated pattern is shown as a solid line, and the difference is shown beneath. The upper tick marks show the *hkl* positions for the nuclear cell, while the lower tick marks show the *hkl* positions for the magnetic cell.

Throughout this work the numbering scheme for both the propagation vectors and the irreducible representations (ireps) follows that developed by Kovalev[35] as these have been recently verified.[36] We note however that the propagation vectors were rotated from the primitive setting used by Kovalev[35] to the conventional $P12_11$ setting.

## III. RESULTS AND DISCUSSION

### A. $NaLaMnWO_6$

The magnetic structure of $NaLaMnWO_6$ provides the natural reference required to understand how the moments of the $Mn^{2+}$ ions order in the absence of other magnetic ions. This compound crystallizes in the monoclinic space group $P2_1$. The lattice parameters of the nuclear structure at 5 K are refined to be $a = 5.5717(3)$ Å, $b = 5.5970(3)$ Å, $c = 8.0155(4)$ Å, and $\beta = 90.225(2)°$. The atomic positions are refined to values that are similar to the room-temperature structure. The reported Néel temperature, $T_N$, of this compound is 10 K.[16] The neutron diffraction pattern taken at ~5 K, in the magnetically ordered phase, shows several additional magnetic peaks that were not present in the pattern taken at 20 K (Fig. 2). These peaks could be indexed with either of the propagation vectors $\boldsymbol{k}_{14} = (\frac{1}{2}, 0, \frac{1}{2})$ or $\boldsymbol{k}_9 = (0, \frac{1}{2}, \frac{1}{2})$. This ambiguity is not surprising considering that the metric symmetry is pseudotetragonal ($a \approx b$). Refinements were carried out for both propagation vectors. While it is not possible to conclusively differentiate between these two $k$ vectors based on the experimental data, the fits obtained when $\boldsymbol{k}_{14} = (\frac{1}{2}, 0, \frac{1}{2})$ were slightly better. Consequently, this propagation vector was chosen for the refinements described below.

TABLE I. Basis vectors for $\boldsymbol{k}_{14}$ with space group $P2_1$. There are no imaginary components to any of the vectors. Atoms 1 and 2 correspond to the Mn at $(\sim 0.75, \sim 0.25, \sim 0.25)$ and $(\sim 0.25, \sim 0.75, \sim 0.75)$, respectively. Nd or Tb atoms 1 and 2 are at $(\sim 0.25, \sim 0.25, \sim 0.5)$ and $(\sim 0.75, \sim 0.75, \sim 0.5)$, respectively. The notation for the $k$ vectors and irreps follows that used by Kovalev (Ref. 35), though the $k$ vectors have been rotated from the primitive setting used by Kovalev to $P12_11$.

| Irrep | Vector | Atom | $\boldsymbol{k}_{14}=(\frac{1}{2},0,\frac{1}{2})$ |
|---|---|---|---|
| $\Gamma_1$ | $\psi_1$ | 1 | 1 0 0 |
| | | 2 | −1 0 0 |
| $\Gamma_1$ | $\psi_2$ | 1 | 0 1 0 |
| | | 2 | 0 1 0 |
| $\Gamma_1$ | $\psi_3$ | 1 | 0 0 1 |
| | | 2 | 0 0 −1 |
| $\Gamma_2$ | $\psi_4$ | 1 | 1 0 0 |
| | | 2 | 1 0 0 |
| $\Gamma_2$ | $\psi_5$ | 1 | 0 1 0 |
| | | 2 | 0 −1 0 |
| $\Gamma_2$ | $\psi_6$ | 1 | 0 0 1 |
| | | 2 | 0 0 1 |

Representational theory is based on decomposing the possible magnetic structures into the irreducible representations of the little group, $G_k$, the subgroup of the crystallographic space group, $G_0$, which leaves the propagation vector invariant. For the space group $P2_1$ $\boldsymbol{k}_{14}=(\frac{1}{2},0,\frac{1}{2})$ is a symmetry point of the Brillouin zone and $G_k$ is identical to $G_0$. There are two magnetic atoms per crystallographic unit cell in this space group. Their magnetic representation, $\Gamma_{mag}$, can be decomposed into two irreps $\Gamma_1$ and $\Gamma_2$ each of order 3. The associated basis vectors are shown in Table I.

RMC refinements were used to explore the possible combinations of basis vectors that could fit the diffraction data. Refinements using only a single basis vector yielded inferior results compared to refinements done with combinations of basis vectors. Refinements using all three basis vectors in $\Gamma_1$ were preformed using the script-clone feature in SARAH which allows for multiple RMC refinements to start the same but develop differently. This allows one to determine which features of a refinement are robust and which are not, an important feature given the information loss associated with powder averaging. Refinements using $\Gamma_1$ provided slightly better fits than when $\Gamma_2$ was used, although the difference was not large enough to conclusively rule out $\Gamma_2$ as a possibility. When ten clones were used the goodness-of-fit $\chi^2$ values for the $\Gamma_1$ refinements ranged from 1.45–1.47 while the $\Gamma_2$ fits ranged from 1.51–1.53. For comparison, the best fit obtained when using the alternate propagation vector of $\boldsymbol{k}_9=(0,\frac{1}{2},\frac{1}{2})$ was $\chi^2=1.68$. The resulting structures from the $\Gamma_1$ refinements consistently had large components in the $x$ and $z$ directions. Removal of the $x$ or $z$ component (refined by setting the contributions from either $\psi_1$ or $\psi_3$ to zero) resulted in a small but significant worsening of the fit. The $y$ component showed significant variation among refinements with essentially the same fits. In some refinements it was nearly zero, while in others it was comparable in magnitude to the $x$ and $z$ components. The $y$ component could be removed ($\psi_2$ set to zero) without degrading the fit. The overall magnitude of the moment was consistently refined to values ranging from 3.92 to 4.00$\mu_B$. The fit to the NPD pattern is shown in Fig. 2.

The structures represented by $\Gamma_1$ and $\Gamma_2$ both correspond to noncollinear spin arrangements. Collinear structures can be constructed by mixing of the two irreps. Refinements using $(\psi_1,\psi_3,\psi_5)$ and $(\psi_2,\psi_4,\psi_6)$ were done to investigate this possibility. The refinement using $(\psi_1,\psi_3,\psi_5)$ gave essentially equal results as fits using $(\psi_1,\psi_2,\psi_3)$. To the simplest approximation the Landau theory of a second-order phase transition requires that only a single irrep is involved in a magnetic ordering transition and, correspondingly, the resulting magnetic structure can be described using a single irrep.[21] Therefore, the noncollinear magnetic structure that is described by a single irrep, $\Gamma_1$, is preferred on symmetry grounds to the collinear structure produced from $\Gamma_1$ and $\Gamma_2$. If the $y$ component of the moment is null then a collinear structure would be obtained that still belongs to a single irrep.

The preferred description is therefore one obtained by refining with only $\psi_1$ and $\psi_3$ since it is both collinear and belongs to a single irrep. This structure is shown in Fig. 3. This structure has moment components of $M_x=3.00(3)\mu_B$, $M_y=0$, and $M_z=2.63(3)\mu_B$ with a total moment of 3.99$\mu_B$. The theoretical moment of $S=5/2$, $d^5$ $Mn^{2+}$ ion is $gS=5\mu_B$, assuming a $g$ factor of 2. The relations between the moments of atom 1 and atom 2 are $M_{x1}=-M_{x2}$, $M_{y1}=M_{y2}$, and $M_{z1}=-M_{z2}$. The moments in this structure all lie within the $xz$ plane.

Rocksalt ordering of magnetic and nonmagnetic $B$-site cations in an ideal perovskite results in a fcc closed packed array of magnetic ions. In many perovskites, such as $NaLaMnWO_6$, tilting of the $BO_6$ octahedra will reduce the symmetry such that the lattice is only pseudo-fcc. In such a structure there are two primary pathways by which superexchange can occur. The first is between the nearest-neighbor (nn) ions connected through a ~90° Mn-O-O-Mn pathway. The second is between next nearest neighbors (nnn) along a ~180° Mn-O-W-O-Mn pathway. In the magnetic structure of $NaLaMnWO_6$ all $Mn^{2+}$ ions which are connected through Mn-O-W-O-Mn nnn pathways are antiparallel, indicating that superexchange through this network of bonds plays an important role in determining the structure. The nn superexchange probably also plays a role in determining the structure but due to the inequivalency of the bond distances (due to the octahedral tilting) the precise details of the exchange are difficult to evaluate. Of the 12 nn $Mn^{2+}$ ions six are parallel and six are antiparallel. This frustration is partly relieved by the monoclinic distortion of the cell. The six nn ions connected along the slightly shorter $a$ axis are the ones which are antiparallel, while the six connected along the slightly longer $b$ axis are the parallel ones.

The magnetic structures of $A_2MnWO_6$ ($A$=Ba,Sr,Ca) perovskites provide a good point of comparison. The only structural difference between these compounds and $NaLaMnWO_6$ is that they lack an ordered arrangement of two different types of $A$-site cations. While ordering of nonmagnetic $A$-site cations is unlikely to have a profound effect

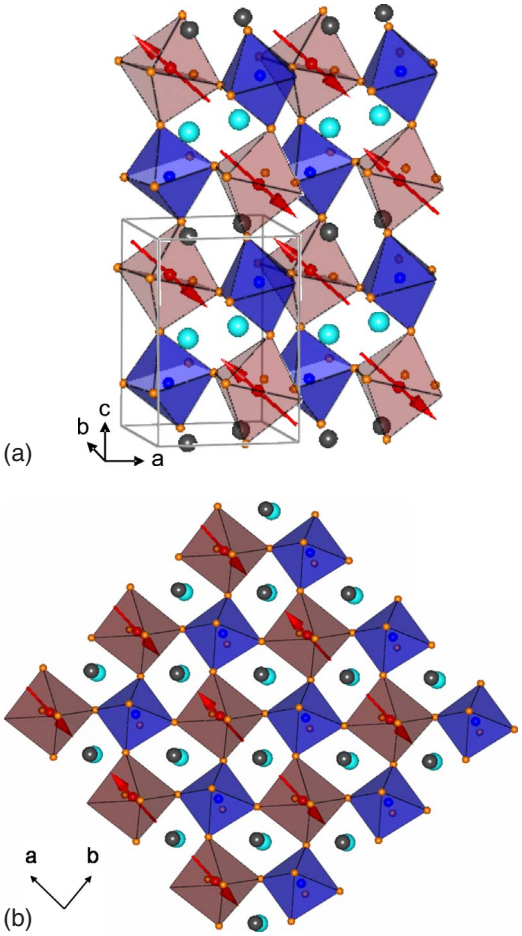


FIG. 3. (Color online) The magnetic structure of $NaLaMnWO_6$. The Mn atoms are shown as red (light gray) spheres surrounded by octahedra. The Mn moments are depicted as arrows. The W atoms are shown as blue (dark gray) spheres surrounded by octahedra. The large teal (light gray) spheres are La atoms, and the large dark gray spheres are Na atoms. Small orange (gray) spheres are oxygen. One magnetic unit cell is shown in the top figure with the box showing one crystallographic unit cell. The lower is a view down the $c$ axis which allows the exchange pathways to be better seen.

on the ordering of the magnetic $B$-site cations, changes in the bond angles and lengths of the corner sharing octahedral network can impact the magnetic structure. The structure of $Ca_2MnWO_6$ has been reported by two separate research groups.[37,38] This compound has the closely related $P2_1/n$ crystallographic symmetry and therefore also has two equivalent positions for the Mn atoms. Both groups found that magnetic ordering occurs according to a propagation vector of $\boldsymbol{k}=(0,\frac{1}{2},\frac{1}{2})$ although they reported different spin arrangements: Azad *et al.*[38,39] reported a collinear spin arrangement, while that of Munoz *et al.*[37] is noncollinear with $M_{x1}=-M_{x2}$, $M_{y1}=M_{y2}$, and $M_{z1}=-M_{z2}$—the same relationship in $NaLaMnWO_6$ as described by $\Gamma_1$. Both groups of researchers have also reported on the structure of $Sr_2MnWO_6$.[37,39] In this case the two reports come to different conclusions regarding the crystallographic space group and therefore different magnetic propagation vectors are reported. Azad *et al.*[38,39] described the symmetry as $P4_2/n$ with $\boldsymbol{k}=(\frac{1}{2},\frac{1}{2},\frac{1}{2})$ while Munoz *et al.*[37] reported that the true

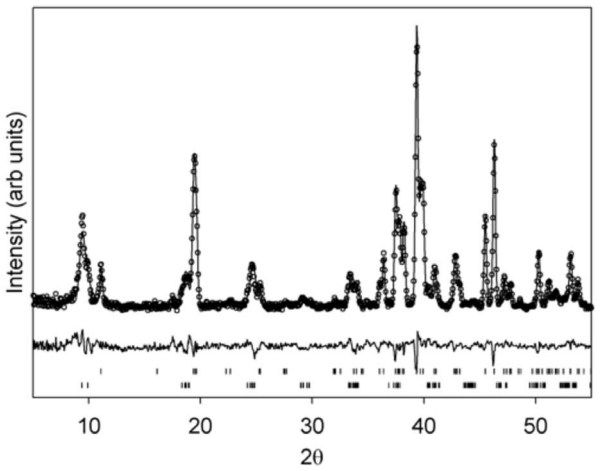


FIG. 4. The neutron powder diffraction pattern of $NaNdMnWO_6$ obtained at 4 K using neutrons of wavelength 1.5403(2) Å. The observed data points are shown as open circles, the calculated pattern is shown as a solid line, and the difference is shown beneath. The upper tick marks show the nuclear reflections, while the lower tick marks show the magnetic reflections.

symmetry is $P2_1/n$ with $\boldsymbol{k}=(\frac{1}{2},0,\frac{1}{2})$. Given the fact that $P2_1/n$ symmetry is the most common space group among $A_2BB'O_6$ perovskites, while examples with $P4_2/n$ are extremely rare, it seems most likely that the latter report is correct.[40] Thus, $Sr_2MnWO_6$ and $NaLaMnWO_6$ appear to adopt the same magnetic structure, while $Ca_2MnWO_6$ adopts a similar structure except that the propagation vector is $\boldsymbol{k}=(0,\frac{1}{2},\frac{1}{2})$ instead of $\boldsymbol{k}=(\frac{1}{2},0,\frac{1}{2})$. The magnetic structure of $Ba_2MnWO_6$ has not been fully determined yet although it is reported to be of a $G$-type arrangement.[41]

### B. $NaNdMnWO_6$

This compound also has $P2_1$ symmetry with lattice parameters of $a=5.4965(2)$ Å, $b=5.5868(2)$ Å, $c=7.9663(2)$ Å, and $\beta=90.364(2)°$ at 4 K. The atomic positions at 4 K are essentially the same as those reported at room temperature. The reported $T_N$ for this compound is 11 K.[16] Below $T_N$ several new peaks appear in the diffraction pattern (see Fig. 4). These peaks could only be indexed by the use of an incommensurate propagation vector, $\boldsymbol{k}_5=(0,u,\frac{1}{2})=(0,0.48,\frac{1}{2})$. For these magnetic positions the little group of the $\boldsymbol{k}_5$ propagation vector contains insufficient symmetry to relate all of the magnetic moments, and the system is cut into orbits that contain the moments either on atom 1 or on atom 2; there is no symmetry relationship between these atoms. The basis vectors resulting from this symmetry are shown in Table II.

When the pattern was refined using the basis vectors associated with $\Gamma_1$ it was found that $\psi_1$ and $\psi_3$ were always refined to small values for the Nd atom. In fact, these components could be removed from the refinement so that only $\psi_2$ was used for Nd and this did not cause any degradation to the fit. The orientation of the Mn moments also seems to be dominated by $\psi_2$; however, the $\psi_1$ and $\psi_3$ components still

TABLE II. Basis vectors for incommensurate $\boldsymbol{k}_5=(0,u,\frac{1}{2})$ propagation vectors in space group $P2_1$. Atoms 1 and 2 refer to the same positions as described in Table I.

| Irrep | Vector | Atom | $\boldsymbol{k}=(0,0.427,\frac{1}{2})$ | $\boldsymbol{k}=(0,0.48,\frac{1}{2})$ |
|---|---|---|---|---|
| $\Gamma_1$ | $\psi_1$ | 1 | 1 0 0+$i$(0 0 0) | 1 0 0+$i$(0 0 0) |
| | | 2 | −0.063 0 0+$i$(−0.998 0 0) | −0.227 0 0+$i$(−0.974 0 0) |
| $\Gamma_1$ | $\psi_2$ | 1 | 0 1 0+$i$(0 0 0) | 0 1 0+$i$(0 0 0) |
| | | 2 | 0 0.063 0+$i$(0 0.998 0) | 0 0.227 0+$i$(0 0.974 0) |
| $\Gamma_1$ | $\psi_3$ | 1 | 0 0 1+$i$(0 0 0) | 0 0 1+$i$(0 0 0) |
| | | 2 | 0 0 −0.063+$i$(0 0 −0.998) | 0 0 −0.227+$i$(0 0 −0.974) |
| $\Gamma_2$ | $\psi_4$ | 1 | 1 0 0+$i$(0 0 0) | 1 0 0+$i$(0 0 0) |
| | | 2 | 0.063 0 0+$i$(0.998 0 0) | 0.227 0 0+$i$(0.974 0 0) |
| $\Gamma_2$ | $\psi_5$ | 1 | 0 1 0+$i$(0 0 0) | 0 1 0+$i$(0 0 0) |
| | | 2 | 0 −0.063 0+$i$(0 −0.998 0) | 0 −0.227 0+$i$(0 −0.974 0) |
| $\Gamma_2$ | $\psi_6$ | 1 | 0 0 1+$i$(0 0 0) | 0 0 1+$i$(0 0 0) |
| | | 2 | 0 0 0.063+$i$(0 0 0.998) | 0 0 0.227+$i$(0 0 0.974) |

appear to be significant and necessary. The best refinement had a $\chi^2$ value of 1.65. This structure has an incommensurate modulation of the moment magnitudes along the $y$ direction. The magnitude of the moments varies sinusoidally along the $b$ axis with a repeat distance of approximately 26 unit cells (~145 Å). The moments on atoms 1 and 2 are in antiphase. In this structure the Nd moments are oriented directly along the $b$ axis with a maximum moment of 3.23(4)$\mu_B$. The theoretical moment for a $Nd^{3+}$ ion is 3.62$\mu_B$. The $Mn^{2+}$ ion has maximum moment components of $M_x$=2.74(2)$\mu_B$, $M_y$=4.67(15)$\mu_B$, $M_z$=2.86(21)$\mu_B$, with a total maximum moment of 6.11$\mu_B$. The large maximal value of the $Mn^{2+}$ moment indicates that there is an additional contribution to the moment of the manganese that could come from the mixing in of excited states or an orbital component, an observation that merits further investigation. We found that the moments of the two ions were not strongly correlated. The structure is shown in Fig. 5.

The experimental diffraction pattern could also be fitted using the basis vectors of $\Gamma_2$. These provided a nearly identical fit as compared to $\Gamma_1$ with the $\chi^2$ of the best fit being 1.62. In this case the $y$ component of the Nd moment was small compared to the $x$ and $z$ components. The Mn moment points mainly along the $y$ direction. The same sinusoidal variation in the magnitude of the moments occurs in the $y$ direction. The maximum moment components for the $Nd^{3+}$ ion are $M_x$=2.03(2)$\mu_B$, $M_y$=1.46(4)$\mu_B$, and $M_z$=2.31(11)$\mu_B$, with a total maximum moment of 3.40$\mu_B$. For the $Mn^{2+}$ ion the maximum moment components are $M_x$=1.64(2)$\mu_B$, $M_y$=5.27(12)$\mu_B$, and $M_z$=1.75(14)$\mu_B$, giving a total maximum moment of 5.79$\mu_B$.

Refinements were also attempted using combinations of basis vectors from both irreps. A $\chi^2$ of 1.63 could be obtained when refining with $(\psi_2,\psi_4,\psi_6)$. Since this fit did not provide any improvement over the refinements done with only a single irrep it was not given further consideration. In the structure obtained using $\Gamma_1$ the Nd moments are collinear, while in the $\Gamma_2$ structure they are not. Of these structures, that corresponding to $\Gamma_1$ appears most likely as the Nd moments lie entirely within the planes of the layers. This result would be consistent with what was found in $NaTbMnWO_6$ as discussed below.

### C. $NaTbMnWO_6$

The nuclear structure of this compound also belongs to space group $P2_1$ with lattice parameters at 11 K of $a$=5.4197(5) Å, $b$=5.5708(4) Å, $c$=7.9073(8) Å, and $\beta$=90.34(1)°. Magnetic susceptibility measurements have indicated that this compound undergoes two magnetic phase transitions upon cooling: a paramagnetic to AF transition occurs at $T_{N1}$~15 K; a second transition occurs at $T_{N2}$~9 K. This second transition appears to be accompanied by some form of canting as the susceptibility begins to increase below this temperature.[16] Neutron powder diffraction spectra were collected at 20, 11, and 6 K. The pattern collected at 20 K shows a broad hump characteristic of short-range magnetic

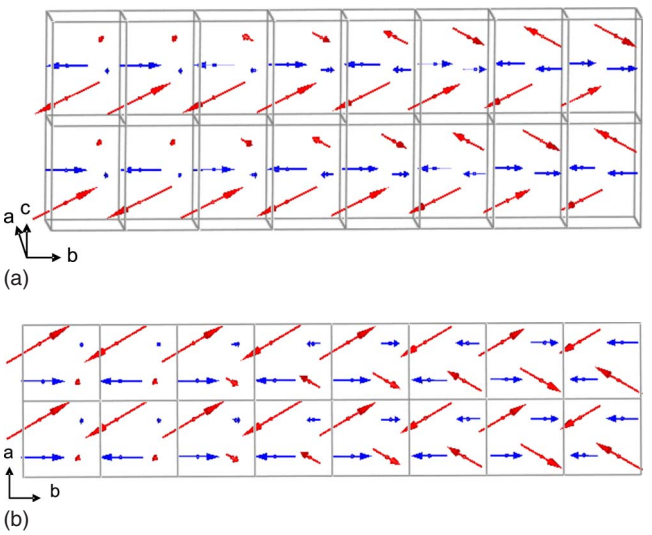


FIG. 5. (Color online) Two views of the magnetic structure of $NaNdMnWO_6$ showing only the magnetic atoms. Red (gray) arrows represent the $Mn^{2+}$ moments, and blue (black) arrows represent the $Nd^{3+}$ moments. Boxes show crystallographic unit cells.

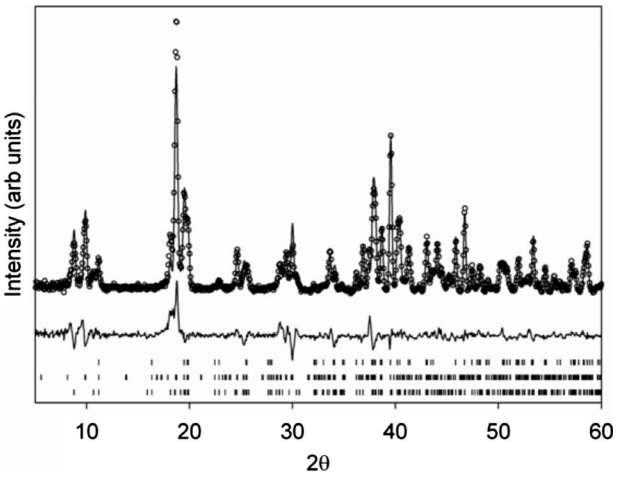


FIG. 6. The neutron powder diffraction pattern of $NaTbMnWO_6$ obtained at 11 K using neutrons of wavelength 1.5403(2) Å. The observed data points are shown as open circles, the calculated pattern is shown as a solid line, and the difference is shown beneath. The upper tick marks are the nuclear reflections, the middle row of tick marks are the reflections arising from the $\boldsymbol{k}_{14}=(\frac{1}{2},0,\frac{1}{2})$ propagation vector, and the lower tick marks show the reflections arising from the $\boldsymbol{k}_5=(0,0.427,\frac{1}{2})$ propagation vector.

order centered around $2\theta=18°$. This is where the strongest magnetic reflections are observed in the 11 and 6 K patterns, indicating that there is still some short-range order at 20 K.

In the neutron powder diffraction pattern taken at 11 K a large number of strong magnetic reflections appear (see Fig. 6). These peaks could not be satisfactorily indexed by a single propagation vector. All the peaks could, however, be accounted for by using two propagation vectors: one commensurate and one incommensurate. The two vectors are $\boldsymbol{k}_{14}=(\frac{1}{2},0,\frac{1}{2})$ and $\boldsymbol{k}_5=(0,u,\frac{1}{2})=(0,0.427,\frac{1}{2})$. Refinements were first attempted by assigning each kind of magnetic ion to a different propagation vector. These refinements were not able to properly account for the peak intensities. The only refinements which gave reasonable results were those that had both magnetic atoms ordering according to both $\boldsymbol{k}_{14}$ and $\boldsymbol{k}_5$—that is to say that both propagation vectors are involved in the spin orderings of both the rare-earth and transition-metal ions. There are two possible explanations for this behavior. One possibility is that there is some degree of phase separation present within the sample. Recent transmission electron microscopy studies of this sample have shown that there are compositional modulations present in some small regions of this sample.[42] The other possibility is that the two vectors correspond to a single phase whose ordering can be described by a commensurate propagation vector which is being modulated by an incommensurate component.

The phase corresponding to $\boldsymbol{k}_{14}$ could be best modeled using the basis vectors of $\Gamma_1$. The moments on both the Mn and Tb atoms lie almost entirely within the *ab* plane. The moments on the Tb are refined to be $M_x=6.02\mu_B$, $M_y=4.23\mu_B$, and $M_z=0.42\mu_B$, giving a total moment of $7.37(14)\mu_B$. The theoretical moment for a $Tb^{3+}$ ion is $9.72\mu_B$. The Mn components are refined to be $M_x=-1.51\mu_B$, $M_y=5.54\mu_B$, and $M_z=0.87\mu_B$, giving a total moment of $5.81(9)\mu_B$. The moment values should be taken with caution since they represent only one component of the total moment. This phase is shown in Fig. 7.

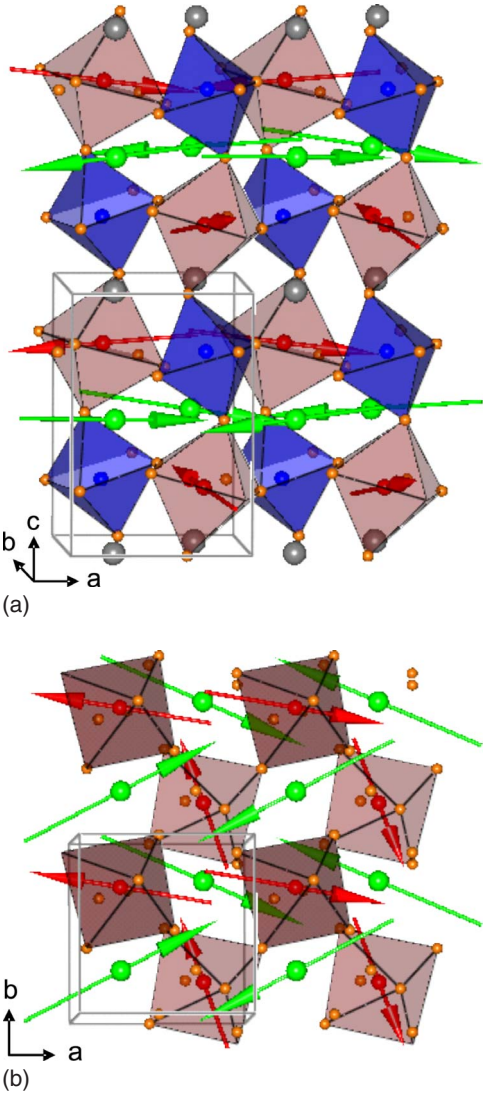


FIG. 7. (Color online) Two views of the structure of the $\boldsymbol{k}_{14}=(\frac{1}{2},0,\frac{1}{2})$ phase of $NaTbMnWO_6$ as refined from neutron powder diffraction data collected at 11 K. The Mn atoms and moments (arrows) are red. The Tb atoms and moments are green. Na is gray, W is blue, and small orange spheres are oxygen. In view of the *ab* plane the Na and W atoms are not shown.

In the structure obtained for the $\boldsymbol{k}_5$ vector the Tb moments lie nearly flat within the *ab* plane similar to the $\boldsymbol{k}_{14}$ structure. Both atoms show a canting which should give a net moment in the *z* direction. The Mn atoms show a much greater canting as they point much more along the *c* axis than the Tb. The orientations of the moments spiral along the *b* axis with a periodicity of approximately seven unit cells (~39.0 Å). The rotation axis of the spiral is the *c* axis. This structure is shown in Fig. 8. The moment values in this phase are much smaller than the theoretical values indicating that this vector represents only a minor component of the moments.

Upon cooling below $T_{N2}$ the neutron diffraction pattern undergoes significant changes (see Fig. 9). The nuclear cell

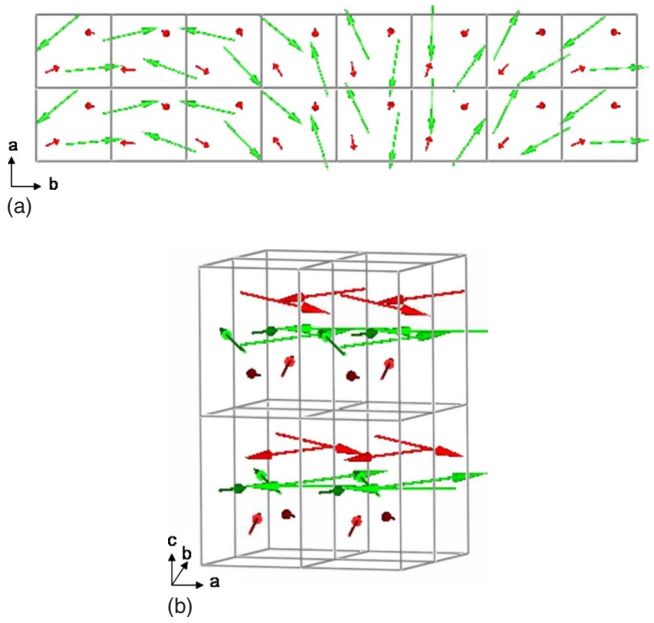


FIG. 8. (Color online) The structure of the $\boldsymbol{k}_5=(0,0.427,\frac{1}{2})$ phase of NaTbMnWO$_6$ at 11 K showing only magnetic atoms. Red (dark gray) shorter arrows represent the $Mn^{2+}$, moments and green (light gray) longer arrows represent the $Tb^{3+}$ moments. Boxes show crystallographic unit cells.

at 6 K has the same lattice parameters, within the uncertainty of the measurement, as those at 11 K. However, the magnetic satellite reflections disappear at the lower temperature and the fundamental reflections increase in intensity. It is now possible to index the pattern using a single propagation vector of $\boldsymbol{k}_{14}=(\frac{1}{2},0,\frac{1}{2})$. The reduction from two propagation vectors to a single $k$ vector favors the idea that the magnetic structure at 11 K is single phase with a magnetic structure which is a superposition of the two propagation vectors.

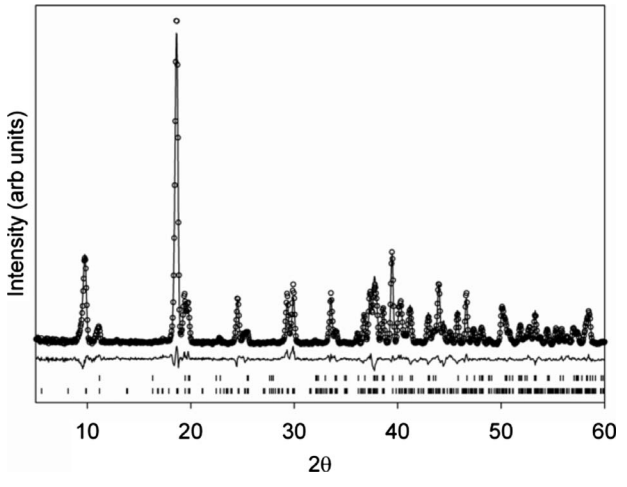


FIG. 9. The neutron powder diffraction pattern of NaTbMnWO$_6$ obtained at 6 K using neutrons of wavelength 1.5403(2) Å. The observed data points are shown as open circles, the calculated pattern is shown as a solid line, and the difference is shown beneath. The upper tick marks show the nuclear reflections, while the lower tick marks show the magnetic reflections.

Upon further cooling the incommensurate modulation disappears.

The best fit to the 6 K data was obtained by using the basis vectors from $\Gamma_1$. The $\chi^2$ for the fit was 2.34. The $z$ component of both Tb and Mn moments could be removed with almost no worsening of the fit. The moments of both atoms lie within the planes of Tb atoms created by the layered ordering. It appears that the two-dimensional layered ordering of the $A$-site cations creates an environment which leads to anisotropic exchange interactions which cause the moments to lie within these planes. Since the NaNdMnWO$_6$ structure shows similar behavior this may be a general feature for this structure type. The $x$ component of the Tb moment is consistently refined to be roughly twice that of the $y$ component. The $y$ component of the Mn moment is also roughly twice that of the $x$ component. This structure (Fig. 10) is similar to that obtained for the same $k$ vector at 11 K; however, the angles between the Tb and Mn moments have changed slightly. The moment components for Tb are $M_x=7.05(6)\mu_B$ and $M_y=3.18(13)\mu_B$ giving a total moment of $7.73\mu_B$. The moment components for Mn are $M_x=2.72(9)\mu_B$ and $M_y=-4.35(12)\mu_B$ giving a total moment of $5.12\mu_B$. These represent small decreases from the 11 K magnetic structure. The larger value of the $Mn^{2+}$ moments in this structure compared to when $L$=La could be attributed to its higher $T_N$ and greater degree of saturation. The NPD pattern of this compound was taken further below its ordering temperature than the other two.

From these results it is also possible to draw conclusions regarding the interactions between the $Mn^{2+}$ and $L^{3+}$ ions. We recently conducted another study on some similar compounds where we replaced $Mn^{2+}$ with $Mg^{2+}$ to form Na$L$MgWO$_6$ perovskites.[43] It was found that these samples remain paramagnetic down to a temperature of 2 K. This is strong evidence that exchange interactions between the $Mn^{2+}$ ions drive the ordering and that the ordering of the $L^{3+}$ lattice is induced by the ordering of the $Mn^{2+}$ lattice. The idea that the Mn sublattice is polarizing the Tb sublattice is further supported by the fact that the two lattices order simultaneously and with the same irrep. From examination of the structure of NaTbMnWO$_6$ it is possible to see how this occurs. Each $Tb^{3+}$ ion is tetrahedrally coordinated by four $Mn^{2+}$ ions. In the $\boldsymbol{k}_{14}$ structures, two of the $Mn^{2+}$ ions form a pair in which the moments are aligned antiparallel to each other. In the second pair of $Mn^{2+}$ ions, which has no symmetry relation to the first, the two moments are aligned parallel to each other. The moment of the $Tb^{3+}$ ion is oriented roughly antiparallel to the pair of parallel $Mn^{2+}$ ions. It appears that the ordering of the $Tb^{3+}$ ions is a result of the local magnetic field created by the ordering of the $Mn^{2+}$ ions. While the $L^{3+}$ ions will not order in the absence of the manganese ions, their presence still appears to have a profound effect on the way in which the $Mn^{2+}$ ions order. In NaTbMnWO$_6$ the moments of the $Mn^{2+}$ ions are all confined to the $xy$ plane just as the $Tb^{3+}$ ions are. This is quite different from what is observed in NaLaMnWO$_6$.

## IV. CONCLUSIONS

We have determined the magnetic structures of three Na$L$MnWO$_6$ compounds. NaLaMnWO$_6$ orders AF at 10 K

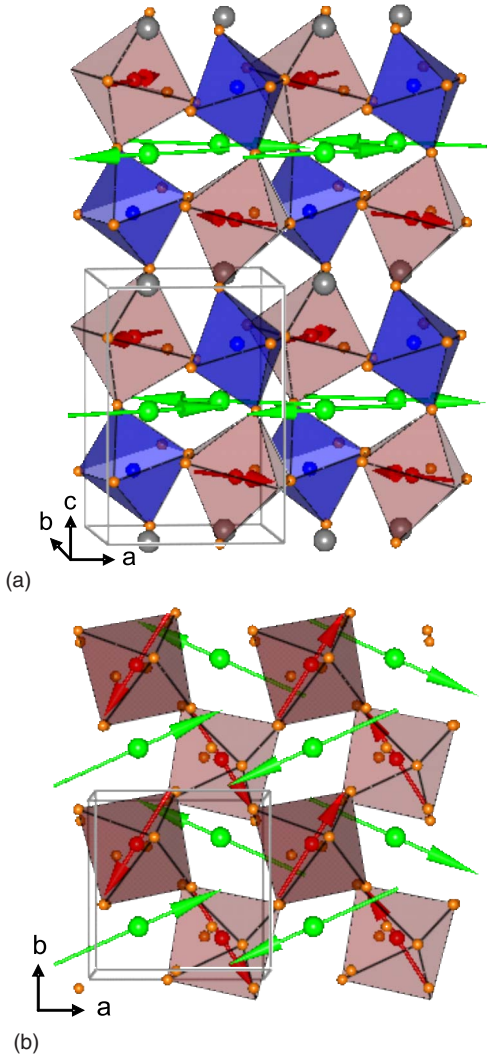


FIG. 10. (Color online) Two views of the magnetic structure of $NaTbMnWO_6$ obtained using powder diffraction data collected at 6 K. Red (dark gray) shorter arrows represent the $Mn^{2+}$ moments, and green (light gray) longer arrows represent the $Tb^{3+}$ moments. Na is gray, W is blue, and small orange spheres are oxygen. The boxes show crystallographic unit cells. In view of the *ab* plane the Na and W atoms are not shown.

with a propagation vector of $k_{14}=(\frac{1}{2},0,\frac{1}{2})$. The moments lie within the *ac* plane with a magnitude of $\sim 4.0\mu_B$ per $Mn^{2+}$. $NaNdMnWO_6$ adopts an incommensurate AF structure at 11 K with a propagation vector of $k_5=(0,u,0.5)=(0,0.48,\frac{1}{2})$. The $Nd^{3+}$ moments point directly along the *b* axis. The magnitude of the moments of both atoms varies along the *b* axis with a repeat distance of ~26 unit cells. $NaTbMnWO_6$ undergoes two magnetic phase transitions at 15 and 9 K. The structure determined at 11 K requires two propagation vectors of $\boldsymbol{k}_{14}=(\frac{1}{2},0,\frac{1}{2})$ and $\boldsymbol{k}_5=(0,0.427,\frac{1}{2})$. The two propagation vectors appear to be describing a complex type of ordering within a single magnetic phase. Upon cooling at 6 K the incommensurate modulation of the moments disappears and the structure is described solely by $\boldsymbol{k}_{14}=(\frac{1}{2},0,\frac{1}{2})$, the same *k* vector used to describe the $NaLaMnWO_6$ structure. The structures corresponding to $\boldsymbol{k}_{14}$ have both Mn and Tb moments confined to the *ab* plane.

One commonality between the magnetic structures of the *L*=Nd and Tb compounds is the observation that the *L* moments are oriented to lie within the *L* layers. This seems to have an important influence on the direction of the manganese moments. In $NaLaMnWO_6$ the Mn moments have a significant component parallel to the *c* axis (perpendicular to the La layers). In contrast to $NaTbMnWO_6$ the Mn moments lie in the *ab* plane parallel to the Tb layers, within experimental error. The Mn moments in $NaNdMnWO_6$ are intermediate.

This study represents the determination of the magnetic structures of $AA'BB'O_6$ perovskites that possess a layered ordering of the *A*-site cations and a rocksalt ordering of *B*-site cations. It has been shown that the interactions between the two magnetic sublattices can lead to complex magnetic structures with features such as incommensurate ordering and multiple magnetic phase transitions. These features coupled with the polar crystal structures of these compounds make them promising candidates for future multiferroics research.

*Note added.* The crystal structures of $NaLaMnWO_6$, $NaNdMnWO_6$, and $NaTbMnWO_6$ at 20, 18, and 20 K, respectively, are available as CIF files.

## ACKNOWLEDGMENTS

Financial support from the NSF through a Materials World Network grant (Grant No. MWN-0603128) and the NSF funded Center for the Design of Materials (Grant No. CHE-0434567) is gratefully acknowledged. We acknowledge the support of the National Institute of Standards and Technology, U.S. Department of Commerce, in providing the neutron research facilities used in this work; and would like to thank Judith Stalick for assistance with the collection of the neutron-diffraction data.

[1] G.-Q. Gong, C. Canedy, G. Xiao, J. Z. Sun, A. Gupta, and W. J. Gallagher, Appl. Phys. Lett. **67**, 1783 (1995).
[2] A. P. Ramirez, J. Phys.: Condens. Matter **9**, 8171 (1997).
[3] J. B. Goodenough and J.-S. Zhou, Chem. Mater. **10**, 2980 (1998).
[4] D. D. Sarma, Curr. Opin. Solid State Mater. Sci. **5**, 261 (2001).
[5] K.-I. Kobayashi, T. Kimura, H. Sawada, K. Terakura, and Y. Tokura, Nature (London) **395**, 677 (1998).
[6] L. I. Balcells, J. Navarro, M. Bibes, A. Roig, B. Martinez, and J. Fontcuberta, Appl. Phys. Lett. **78**, 781 (2001).
[7] J. Wang, *et al.*, Science **299**, 1719 (2003).
[8] T. Kimura, S. Kawamoto, I. Yamada, M. Azuma, M. Takano, and Y. Tokura, Phys. Rev. B **67**, 180401(R) (2003).
[9] W. Eerenstein, N. D. Mathur, and J. F. Scott, Nature (London)

**442**, 759 (2006).
[10] C. N. R. Rao and C. R. Serrao, J. Mater. Chem. **17**, 4931 (2007).
[11] D. I. Khomskii, J. Magn. Magn. Mater. **306**, 1 (2006).
[12] T. Kimura, T. Goto, H. Shintani, K. Ishizaka, T. Arima, and Y. Tokura, Nature (London) **426**, 55 (2003).
[13] R. Kajimoto, H. Yoshizawa, H. Shintani, T. Kimura, and Y. Tokura, Phys. Rev. B **70**, 012401 (2004).
[14] T. Goto, T. Kimura, G. Lawes, A. P. Ramirez, and Y. Tokura, Phys. Rev. Lett. **92**, 257201 (2004).
[15] M. C. Knapp and P. M. Woodward, J. Solid State Chem. **179**, 1076 (2006).
[16] G. King, S. Thimmaiah, A. Dwivedi, and P. M. Woodward, Chem. Mater. **19**, 6451 (2007).
[17] http://www.ncnr.nist.gov/
[18] A. S. Wills, Physica B **276–278**, 680 (2000); program available at www.ccp14.ac.uk
[19] A. S. Wills, arXiv:0905.0873v1 Z. Kristallogr. (to be published).
[20] J. R. Stewart, A. S. Wills, C. J. Leavy, B. D. Rainford, and C. Ritter, J. Phys.: Condens. Matter **19**, 145291 (2007).
[21] J. Rossat-Mignod, *Methods of Experimental Physics: Neutron Scattering* (Academic Press, New York, 1987), Vol. 3.
[22] A. S. Wills, Z. Kristallogr. **26**, 53 (2007).
[23] E. F. Bertaut, J. Appl. Phys. **33**, 1138 (1962).
[24] E. F. Bertaut, Acta Crystallogr., Sect. A: Cryst. Phys., Diffr., Theor. Gen. Crystallogr. **24**, 217 (1968).
[25] E. F. Bertaut, J. Phys. Colloq. **C1**, 462 (1971).
[26] E. F. Bertaut, J. Magn. Magn. Mater. **24**, 267 (1981).
[27] C. J. Bradley and A. P. Cracknell, *The Mathematical Theory of Symmetry in Solids* (Clarendon Press, Oxford, 1972).
[28] A. Lappas, A. S. Wills, M. A. Green, K. Prassides, and M. Kurmoo, Phys. Rev. B **67**, 144406 (2003).
[29] A. S. Wills, Phys. Rev. B **63**, 064430 (2001).
[30] A. S. Wills, M. Zhitomirsky, B. Canals, J. P. Sanchez, P. Bonville, P. Damlas de Réotier, and A. Yaouanc, J. Phys.: Condens. Matter **18**, L37 (2006).
[31] A. Poole, A. S. Wills, and E. Lelièvre-Berna, J. Phys.: Condens. Matter **19**, 452201 (2007).
[32] A. C. Larson and R. B. Von Dreele, general structure analysis system (GSAS), Los Alamos National Laboratory Report No. LAUR 86–748, 2004 (unpublished).
[33] B. H. Toby, J. Appl. Crystallogr. **34**, 210 (2001).
[34] J. Rodriguez-Carvajal, Physica B **192**, 55 (1993).
[35] O. V. Kovalev, *Representations of the Crystallographic Space Groups*, 2nd ed. (Gordon and Breach Science Publishers, Switzerland, 1993).
[36] Z. L. Davies and A. S. Wills, J. Phys.: Condens. Matter **20**, 104232 (2008).
[37] A. Munoz, J. A. Alonso, M. T. Casais, M. J. Martinez-Lope, and M. T. Fernandez-Diaz, J. Phys.: Condens. Matter **14**, 8817 (2002).
[38] A. K. Azad, S. A. Ivanov, S.-G. Eriksson, J. Eriksen, H. Rundlof, R. Mathieu, and P. Svedlindh, Mater. Res. Bull. **36**, 2485 (2001).
[39] A. K. Azad, S. A. Ivanov, S.-G. Eriksson, H. Rundlof, J. Eriksen, R. Mathieu, and P. Svedlindh, J. Magn. Magn. Mater. **237**, 124 (2001).
[40] M. W. Lufaso, P. W. Barnes, and P. M. Woodward, Acta Crystallogr., Sect. B: Struct. Sci. **62**, 397 (2006).
[41] A. K. Azad, S. A. Ivanov, S.-G. Eriksson, J. Eriksen, H. Rundlof, R. Mathieu, P. Svedlindh, Mater. Res. Bull. **36**, 2215 (2001).
[42] S. Garcia-Martin, G. King, and P. M. Woodward (unpublished).
[43] G. King, L. M. Wayman, and P. M. Woodward, J. Solid State Chem. **182**, 1319 (2009).